Effect of Initial Residual Stress and Machining-Induced Residual Stress on the Deformation of Aluminium Alloy Plate

Xiaoming Huang[1] – Jie Sun[1,2,*] – Jianfeng Li[1,2]

[1] Shandong University, School of Mechanical Engineering, China
[2] Ministry of Education, Key Laboratory of High Efficiency and Clean Mechanical Manufacture, China

During the machining of aerospace thin-walled components, a large amount material is removed, and machining-induced residual stress is induced in the boundary layer of the work piece, which results in deformation of the components. In this study, the effects of material initial residual stress and machining-induced residual stress on the deformation of aluminium alloy plate are studied. A theoretical model of the plate is analysed first, and the experiments of the milling deformation under different initial residual stress conditions are performed. The results show that the machining-induced residual stress is the primary factor of distortion. The coupling action of compressive initial residual stress and machining-induced residual stress increase the plate deformation, and the coupling action of tensile initial residual stress and machining-induced residual stress decrease the plate deformation. The finite element simulation results are compared with experimental results and found to be in good agreement.
Keywords: thin walls, machining distortion, residual stress, chemical milling

Highlights
- *Machining deformation mechanism of plate was studied.*
- *Analysis of deformation factors weights.*
- *The effect of the plate initial residual stress on the magnitude of the deformation.*
- *Studied the relationships between the maximum deflection and the thickness of the specimens.*

0 INTRODUCTION

With increasing demand for the improvement of airplane performance, large monolithic components are widely used in order to reduce airplane weight in the aviation industry [1]. During the machining process of structural components, up to 90% of the material is removed from the blank. For those components, it is easy to cause substantial distortion because of the initial residual stress and machining-induced residual stress.

Aircraft parts are typically machined from pre-stretched 7050-T7451 aluminium alloys. In order to reduce the initial residual stresses and increase mechanical strength, pre-treatments are performed in producing blank plates, i.e. quenching, extrusions, stretching, etc. [2] and [3]. However, it is difficult to eliminate the initial stress. Machining-induced residual stress is produced on the machined surface of the work piece due to the action of machining.

In order to control the thin-walled component deformation, some investigations have been done. Rai and Xirouchakis studied the milling thin-walled component distortion based on an FEM machining environment [4]. An FEM method called "house-building frame modelling" was used to predict the milling distortion of monolithic aero-component under different milling conditions [5]. For this study, machining loads were used to replace the machining-induced residual stresses, and initial residual stresses were ignored. This assumption is inappropriate for the actual situation.

Assuming that stresses induced by the machining process were negligible, Sun and Ke studied the influence of initial residual stress on the machining distortion of large unitization airframes [6]. Huang et al. investigated the effects of the milling process sequence on the deformation of frame monolithic components by establishing cutting force fields and temperature fields [7]. Moreover, some studies on monolithic component deformation were focussed on surface dimensional error caused by machining load and clamping force [8] and [9].

Although some studies have been done to analyse the machining distortion, there is a lack of comprehensive studies on the cause and primary effect element of machining distortion of thin-walled components. The joint action of initial residual stress and machining-induced residual stresses on thin-walled component deformation has not been fully explored, and fundamental research is required to understand how machining distortion develops.

In this paper, machining residual stress is induced by the high-speed milling thin-walled plates of

different locations in 60 mm thick 7050-T7451 plates, which are used to explore the effect of machining-induced residual stress and blank initial residual stress for deformation. In order to avoid introducing additional stress, chemical milling experiments are conducted to thin the specimens gradually.

1 THEORETICAL ANALYSIS MODEL

For a simple rectangular block, there are only longitudinal residual stresses in the transverse directions along the thickness, as shown in Fig. 1. It is assumed that the material is removed without creating residual stresses at the exposed material surface [10]. Because there are no external forces acting on the plate, all forces and bending moment acting over any cross-section of the plate must be in equilibrium before and after the materials were removed:

$$\int \sigma dA = 0, \quad \int dM = 0. \tag{1}$$

The relationship between the moment and curvature change is given by [6]:

$$\frac{1}{\rho_m} - \frac{1}{\rho_{m+1}} = \frac{6\delta\delta_m\sigma_{j1}}{E(\delta_{m+1})^3}, \tag{2}$$

where, ρ_m/ρ_{m+1} are radii of curvatures of the mid-section of the remaining body, before and after removal of the mth layer; δ is the thickness of the removed layer; δ_m and δ_{m+1} are the height of the body before and after the removal of the mth layer; E is Young's modulus, and σ_{j1} is the residual stress of the mth layer before it is removed.

Since the distribution of the residual stress in the remaining body is changed due to the removal of the mth layer, the curvature change resulting from the removal of the $(m+1)$th layer will be a function of the new state of residual stress as opposed to the original state of residual stress.

The shaded triangle shown in Fig. 1 represents the stress state in the block that is created by bringing the remaining body back to its equilibrium state.

$$\sigma_{j1}\delta + \frac{h_{um}S_m}{2} + \frac{h_{lm}S_m'}{2} = 0, \quad j = m-1, \tag{3}$$

where, h_{um} and h_{lm} are the height from the neutral axis to the upper and bottom surface of the remaining body, S_m and S_m' are stresses that are produced at the upper and bottom surfaces of the remaining body.

The relationship between the stress S_m and the curvature change caused by the removal of the mth layer can be expressed as:

$$S_m = h_{um}E(\frac{1}{\rho_m} - \frac{1}{\rho_{m+1}}). \tag{4}$$
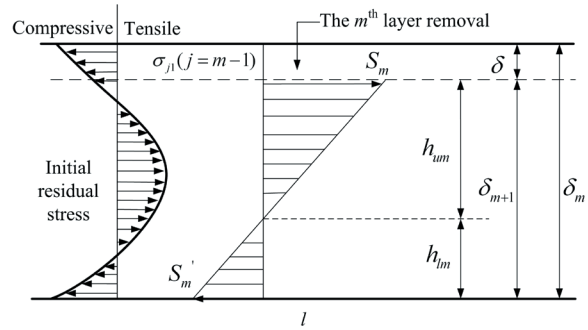
Fig. 1. *Initial residual stress and additional stresses after the removal of materials*

Referring to Fig. 1,

$$h_{um} + h_{lm} = \delta_{m+1}, \tag{5}$$

$$S_m' = (h_{lm} / h_{um})S_m, \tag{6}$$

Utilizing Eqs. (2) through (6),

$$h_{um} = \frac{\delta_{m+1}(3\delta_m + \delta_{m+1})}{6\delta_m}. \tag{7}$$

In order to compute the stress σ_{j1}, the correction terms accounting for the removals of the first layer through the mth layer should be calculated. For computing the correction terms, the stress, S_k for $1 < k < j$, which would be produced by bringing back the remaining body after the removal of the kth layer to the shape prior to the removal of the kth layer, should be first determined.

$$\begin{aligned} \sigma_{11} &= \sigma_2 - S_{11}, \\ \sigma_{21} &= \sigma_3 - (S_{12} + S_{22}), \\ \sigma_{31} &= \sigma_4 - (S_{13} + S_{23} + S_{33}), \\ &\vdots \quad . \end{aligned} \tag{8}$$

In general, Eq. (8) can be written as:

$$\sigma_{j_1} = \sigma_{j+1} - \sum_{m=1}^{j} S_{mj}. \tag{9}$$

In the actual milling process, machining-induced residual stresses are brought to the new surface of the work piece, which affect the deformation of the thin-walled plate coupling with the initial residual stress. The closed-form solutions developed in this section for computing the curvature of the known original residual stress can be solved with Matlab software.

2 EXPERIMENTS

2.1 Experiment Specimens

The investigation is performed on 7050-T7451 alloy. The mechanical properties of the material are shown in Table 1.

Table 1. *Mechanical properties of 7050-T7451*

Modulus of Elasticity	Tensile Yield Strength	Shear Strength	Density
71.7 GPa	469 MPa	303 MPa	2.83 g/mm³

Four specimens of altered position in the 60 mm thickness 7050-T7451 aluminium sheet are studied. Specimen position is shown in the Fig. 2a, and specimen IV is in the middle of the thickness direction. The interval distance is 7 mm, and the plate thickness is 2 mm. The initial residual stress of Specimens I and III are tensile, Specimen II is compressive, and Specimen IV lies in the centre of the blank. The size of the specimen is 140×50×2 mm; the length, width, and height directions are parallel, perpendicular pre-stretched direction and thickness direction.
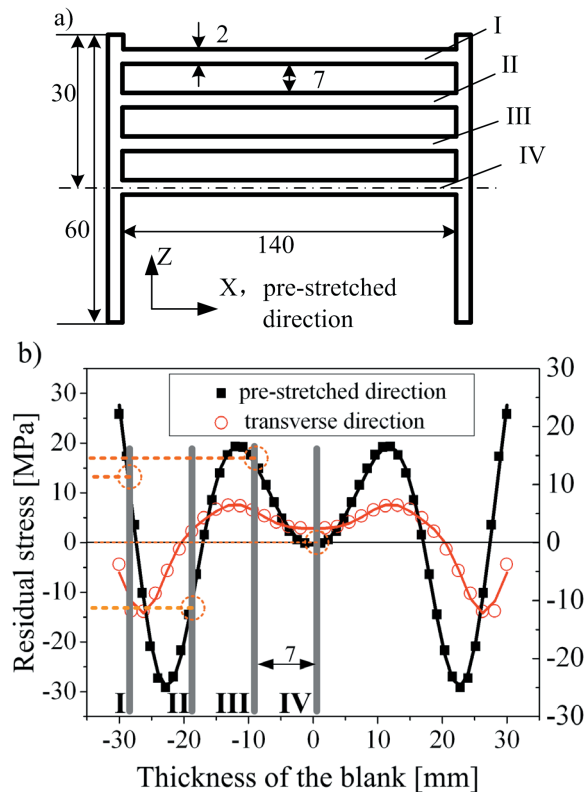
Fig. 2. *Specimen position and the initial residual stress profile of 7050-T7451 plate*

In order to obtain the initial residual stress profile, a crack-compliance method was used to measure the original residual stress [11]. Fig. 2b shows the initial residual stress distribution profile along thickness direction in the blank.

2.2 Milling Induced Residual Stress

Machining residual stresses are introduced by high-speed milling; the milling test is performed on a DECKEL MAHO DMU 70V five-axis universal machining centre, and the tool used is an end mill without coating. The detailed values of the experimental conditions are presented in Table 2.

Table 2. *The experimental conditions*

CNC	DECKEL MAHO DMU 70V 5-axis universal machining centre	
Tool	Material	Solid cemented carbide
Machining state	Dry, Down milling	
Machining parameters	v	628 m/min
	fz	0.06 mm
	a_p	5 mm
	a_e	12 mm

Specimen IV is shown in Fig. 3a; x denotes the perpendicular feed direction.
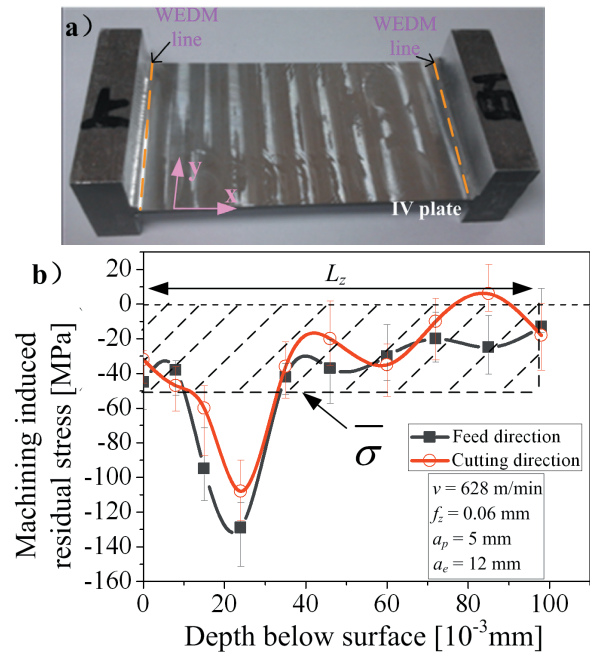
Fig. 3. *Specimen and machining-induced residual stresses profiles of 7050-T7451 thin-walled plate*

The plates are cut down by wire electrical discharge machining (WEDM), which leaves a heat affected zone (HAZ). The research shows that the HAZ has a thickness of the order of microns [12] and [13], which is much less than the specimen size (140×50 mm). It is assumed that the WEDM induced the residual stress but did not influence the initial residual stress distribution and plate deformation.

The machining-induced residual stress on the surface of the work piece is measured using X-ray diffraction technique and electro-polishing technology [14], which is shown in Fig. 3b.

2.3 Chemical Milling

In order to reduce the introduction of additional stresses, chemical milling is used to remove materials gradually from one side of the plate. The composition and ratio of the chemical milling fluid are shown in Table 3. A chemical milling protective coating (HH968-2) is used to ensure that the machining-induced residual stress is unbroken on one side of the surface.

Table 3. *The primary composition and ratio of chemical milling fluid*

NaOH(g)	Na$_2$S(g)	TEA(g)	H$_2$O(g)	NaOH(g/L)
175	18	33	678	180

An increasing amount of material is chemically removed from the surface of the four specimens. Specific thicknesses of the plate can be seen in Table 4. Before and after the chemical milling of each specimen, the thicknesses of the thin-walled plates are measured using a micrometer.

Table 4. *Incremental chemical milling and plate thickness*

Initial thickness [mm]	2	1.75	1.5	1.25	1
Thickness after chemical milling [mm]	1.75	1.5	1.25	1	0.75
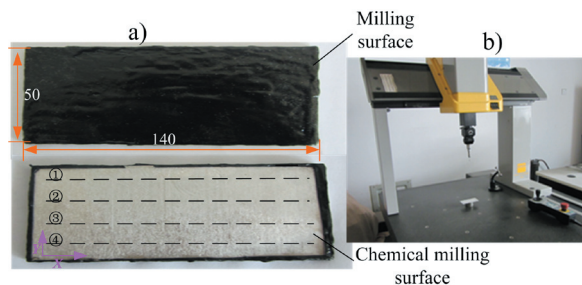
Fig. 4. *Chemical milled sample and deformation measurement*

The distortion values of characteristic points of machined thin-walled plate are measured using a MISTRAL 775 3D coordinate-measure-machine, as shown in Fig. 4. Four characteristic lines are setup along the X direction on the chemical milling surface as shown in Fig. 4a, and some characteristic points along the characteristic lines are picked up at intervals.

The distortion values of characteristic points of machined thin-walled plate are measured using a MISTRAL 775 3D coordinate-measure-machine, as shown in Fig. 4. Four characteristic lines are setup along the x direction on the chemical milling surface as shown in Fig. 4a, and some characteristic points along the characteristic lines are picked up at intervals.

3 RESULTS AND DISCUSSION

The deformations are graphed by the average value of the four characteristic lines. The measurements results for a 0.75 mm thickness plate are presented in Fig. 5. It can be seen that the specimens exhibit significant bowing. The thin-walled plates present convex and bending distortions, with the law of symmetric distribution from the middle to two sides. The convex directions of specimens with initial compressive and tensile stress are the same. Machining-induced residual stress results in the machined side facing up.
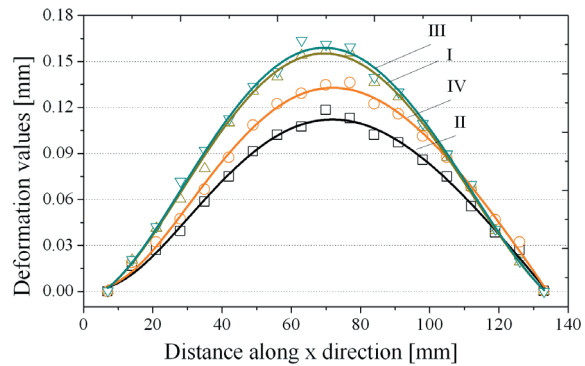
Fig. 5. *Specimen deformation of 0.75 mm thickness plate*

The deformation degree of the four specimens is shown as: III>I>IV>II. Specimen IV's deformation is considered to be caused by machining-induced residual stress, mostly because of its location and the initial residual stress profile. For Plates I and III, the coupling effect of tensile initial residual stress and machining-induced residual stress increases the deformation compared with Plate IV. For Plate II, the coupling effect of the compressive initial residual stress and the machining-induced residual stress decrease the deformation, in comparison with Plate IV.

The relationships of the maximum deflection and the thickness of the four specimens are shown in Fig. 6. As can be seen, the non-linear deformation increases gradually when the materials are removed from one side. The residual stress has a significant impact on the deformation of plates of different thicknesses. This 1.75 mm plate is 2.3 times the thickness of that 0.75 mm one, and the 0.75 mm plate deformation is approximately 9.8 times that of the 1.75 mm plate deformation. According to the curve of Fig. 6, the curve slopes at different thickness are calculated and listed in Table 5. Deformation differentiation of the four plates is not significant when the thickness is more than 1.5 mm. When the thickness is less than 1.25 mm, the machining-induced residual stress has a greater effect on the plate deformation.
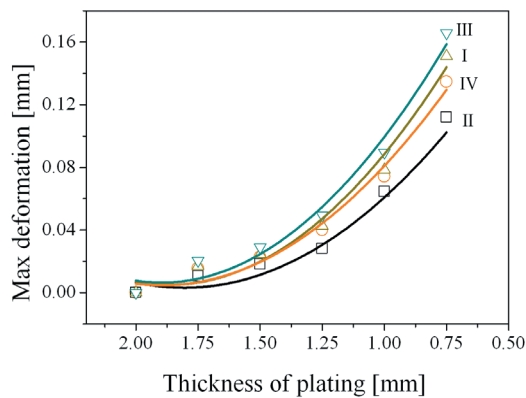
Fig. 6. *The relationship of max deformation and thin-walled plate thickness*

The max displacements of the four specimens are 0.151, 0.112, 0.165 and 0.134 mm when the thickness is 0.75 mm. The influence of the initial stress on deformation is (0.165–0.112) mm = 0.053 mm, which accounts for about one third of the total deformation. Machining-induced residual stress is the primary effect element of machining distortion for the 0.75 mm thick aluminium alloy plate.

Table 5. *Deformation slope at different thicknesses*

Plate thickness [mm]	1.75	1.5	1.25	1.0	0.75
I	0.048	0.051	0.010	0.247	0.350
II	0.041	0.045	0.107	0.154	0.213
III	0.057	0.057	0.121	0.277	0.393
IV	0.045	0.048	0.103	0.175	0.218

4 FEM SIMULATION

Finite element simulation of machining distortion is performed using the ABAQUS commercial finite element software. The size of the thin-walled plate is the same as that of the experimental specimen (140×50×2 mm). The model was meshed with the C3D8R element, with a total of 1120 elements and 1512 nodes.

The residual stress curve from Fig. 2b is dispersed, and the corresponding value of the residual stress at each position was assumed to act uniformly through the thickness of the thin-wall plate, as shown in Fig. 2b. The initial residual stress of every plate is applied to the finite element model using the corresponding node command in FEM.

The arithmetic mean stress ($\overline{\sigma}$) in the machining affected zone (0.1 mm) is obtained in order to characterize the machining-induced residual stress according to the following calculation:

$$\overline{\sigma} = \frac{\int_0^z \sigma \, dz}{L_z}, \qquad (10)$$

where, L_z is the upper limit of integration, which is shown in Fig 3b. The results are computed using Origin 8.0 commercial software.

The machining-induced residual stress data is applied to the milling affected zone. Via the superposition of initial residual stresses and machining-induced stress, combined deformation effects can be determined. The task is to define the complete stress tensor (pre-stretched direction and transverse direction) at each node, and to have it for the complete model in mechanical equilibrium.

The technology of "element birth and death" was used to simulate the chemical milling process in the software, in which the stiffness matrix multiplied by a very small coefficient to deactivate the element (usually it is set to zero); simultaneously, the quality, damp, and specific heat were all set to zero.

For finite element simulation, the thickness was divided into 8 equal layers of 0.25 mm each, with the simulation of the machining process (one removal at a time) representing a 0.25 mm reduction in thickness of the plate.

The 3-2-1 constraint principle was adopted as the boundary conditions, where the rigid motion of the work piece was constrained, but the work piece can be free to distort to reach a new stress equilibrium state.

The deformation nephogram of Plate I at 0.75 mm thickness is shown in Fig. 7a, and the Mises stress redistribution along the thickness direction is shown in Fig. 7b. The distortion law from the finite element simulation accords with the experimental result, which reveals a bending distortion in the middle and warped
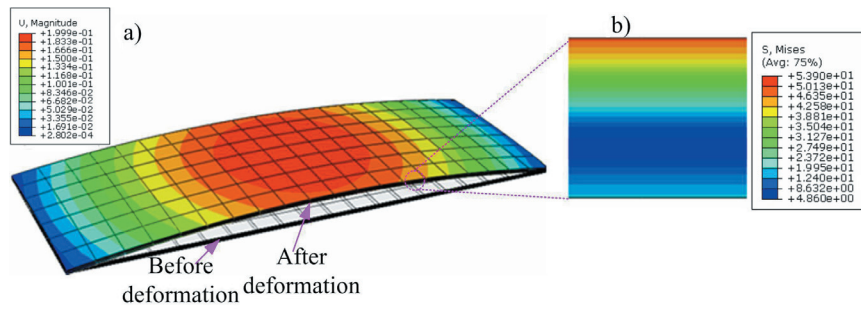
Fig. 7. *Deflection and residual stress redistribution of thin-walled plate I (0.75 mm)*

at both ends. As can be seen, the max deflection is in the plate central part. The machining-induced residual stress is on the convex surface. The max displacement and Mises stress are 0.199 mm and 53.9 MPa in machining surface.

stress has uniform distribution because of the milling tool-path; measurement precision; calculation error, etc. The maximal error is 29.8%, which is in the acceptable range.
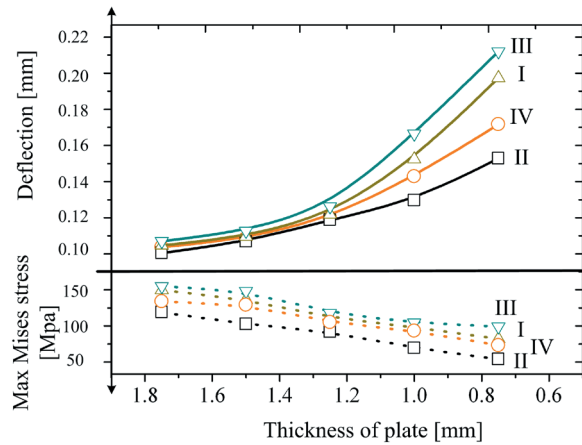
Fig. 8. *The maximum deformation and Mises stress of thin-walled plate thickness*
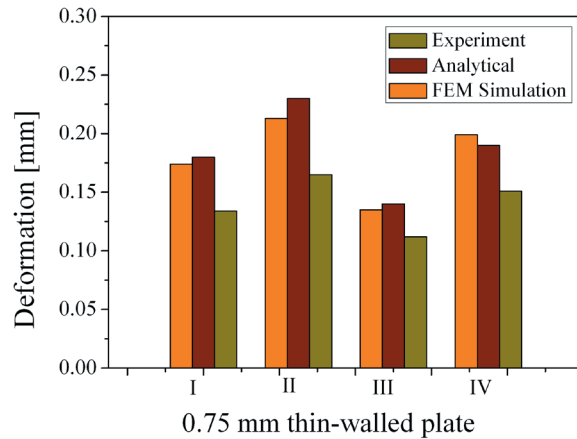
Fig. 9. *The max deformation of FEM analytical and experiments results*

The FEM simulation results of maximum Mises stress and the corresponding deformations are shown in Fig. 8. As the materials are removed, the maximum surface Mises linearly decreased, and the maximum deflection nonlinearly increased. Moreover, the finite element simulation and experiment have the same deformation degree: III>I>IV>II. The order of max Mises stress is III>I>IV>II, which is the same as the deflection order.

The maximum deformation of the FEM simulation, as well as analytical and experiments results are shown in Fig. 9. As can be seen, the theoretical calculation result has good agreement with the FEM. The maximum margin of error between FEM and analytical value was 7.9%. The experimental values are less than the FEM results. There are some error factors producing the difference between FEM and experimental results: machining-induced residual

5 CONCLUSIONS

The effects of material initial residual stresses and machining-induced residual stresses on the deformation of aluminium alloy plate are studied. The thin-walled specimens appeared convex and bending distortion, and machining induced residual stress result in the machined side facing up. The machining-induced residual stress is the primary cause of plate deformation.

The location of the plate has some effect on the magnitude of the deformation. Compared with the near center plate, the deformation is greater when the plate is in the tensile residual stress zone of the blank, and the deformation is lesser when the plates are in the compressive residual stress zone of the blank. The relationships of the maximum deflection and the thickness of the specimens are studied, and the results

show that the machining-induced residual stress has a greater effect on the plate deformation when the thickness is below than 1.25 mm.

The tendency of FEM deformation is consistent with the experiment results, and the values are greater than the measurement values. As the materials are removed, the max Mises stress decreased almost linearly.

6 ACKNOWLEDGEMENTS

7 REFERENCES

[1] Megson, T.H.G. (2012). *Aircraft Structures for Engineering Students*. Leeds University, Leeds.

[2] Li, P.Y., Xiong B.Q., Zhang, Y.A., Li, Z.H. (2012). Temperature variation and solution treatment of high strength AA7050. *Transactions of Nonferrous Metals Society of China,* vol. 22, no. 3, p. 546-554, **DOI:10.1016/S1003-6326(11)61212-0**.

[3] Burtchen, M., Hunkel, M., Lübben, Th., Hoffmann, F., Zoch, H.-W. (2009). Simulation of Quenching Treatments on Bearing Components. *Strojniški vestnik - Journal of Mechanical Engineering*, vol. 55, no. 3, p. 155-159.

[4] Rai, J.K., Xirouchakis, P. (2008). Finite element method based machining simulation environment for analyzing part errors induced during milling of thin-walled components. *International Journal of Machine Tools and Manufacture*, vol. 48, no. 6, p. 629-643, **DOI:10.1016/j.ijmachtools.2007.11.004**.

[5] Guo, H., Zuo, D.W., Wu, H.B. Xu, F. Tong, G.Q. (2009). Prediction on milling distortion for aero-multi-frame parts. *Materials Science and Engineering A*, vol. 499, no. 1, p. 230-233, **DOI:10.1016/j.msea.2007.11.137.**

[6] Sun, J., Ke, Y.L. (2005). Study on machining distortion of unitization airframe due to residual stress. Chinese Journal of Mechanical Engineering, vol. 41, no. 2, p. 117-122, **DOI:10.3901/JME.2005.02.117**. (in Chinese)

[7] Huang, Z.G., Ke, Y.L., Dong, H.Y. (2005). Finite element model of milling process sequence for frame monolithic components. *Journal of Zhejiang University (Engineering Science)*, vol. 39, no. 3, p. 368-372. (in Chinese)

[8] Ratchev, S., Huang, W., Liu. S., Becker, A.A. (2004). Modelling and simulation environment for machining of low-rigidity components. *Journal of Materials Processing Technology*, vol. 153-154, p. 67-73, **DOI:10.1016/j.jmatprotec.2004.04.301**.

[9] Abdullah, R. (2011). *Hybrid Deflection Prediction for Machining Thin-Wall Titanium Alloy Aerospace Component*, Ph.D. Thesis, RMIT University, Melbourne.

[10] Shang, H.S. (1995). *Prediction of the Dimensional Instability Resulting from Machining of Residually Stressed Components*, Ph.D. thesis, Texas Tech University, Lubbock.

[11] Prime, M.B., Hill, M.R. (2002). Residual stress, stress relief and inhomogeneity in aluminum plate. Scripta Materialia, vol. 46, no. 1, p. 77-82, **DOI:10.1016/S1359-6462(01)01201-5**.

[12] Izquierdo, B., Plaza, S., Sánchez, J.A., Pombo, I., Ortega, N. (2012). Numerical prediction of heat affected layer in the EDM of aeronautical alloys. Applied Surface Science, vol. 259, p. 780-790, **DOI:10.1016/j.apsusc.2012.07.124**.

[13] Banerjee, S., Prasad, B.V.S.S., Mishra, P.K. (1997) Analysis of three-dimensional transient heat conduction for predicting wire erosion in the wire electrical discharge machining process. *Journal of Materials Processing Technology*, vol. 65, no. 1-3, p. 134-142, **DOI:10.1016/0924-0136(95)02253-8**.

[14] Huang, X.M., Sun, J., Li, J.F., Han, X., Xiong, Q.C. (2013). An experimental investigation of residual stresses in high-speed end milling 7050-T7451 Aluminum alloy. *Advances Mechanical Engineering*, vol. 2013, Article ID 592659, **DOI:10.1155/2013/592659**.